CHAPTER 7

Kinetic Modelling and Extraction of Metabolic Parameters

H. Herzog[a*], H. Iida[b,c] and L. Caldeira[a]

a Forschungszentrum Jülich, Institute of Neurosciences and Medicine – 4, D-52425 Jülich, Germany

b Department of Investigative Radiology, National Cerebral and Cardiovascular Centre, Osaka, Japan

c Department of Medical Physics, Turku University Hospital, Department of Biomedicine, University of Turku, Turku, Finland

***Corresponding contributor. E-mail: h.herzog@fz-juelich.de**

Abstract

Using molecules radiolabelled with positron emitters PET imaging provides information about a multitude of physiological and metabolic functions. The primary PET images give a qualitative insight into these functions. When PET images and data of the time course of the PET radiopharmaceutical in the blood are combined in an appropriate biological model the extraction of quantified parameters of the observed function becomes possible. This chapter gives an introduction into the kinetic modelling with PET and the related mathematical procedures. It describes some basic and often used applications. Finally, it indicates the application of kinetic modelling in case of MR-PET.

7.1 Introduction

While MRI is considered primarily as a tool to image anatomical details with high resolution, PET can be characterized as the tracer method to observe physiological and metabolic functions without any disturbance by the measurement. Often just a qualitative image of the uptake of the radiotracer labelled with a positron emitter gives sufficient information about a disease. This is demonstrated in Fig. 7.1 where the lacking uptake of [^{18}F]fluoro-deoxyglucose (FDG) in the occipito-temporal cortex gives a clear hint towards Alzheimer's disease. However, if you ask whether the radiotracer uptake of whole organ is too low, a just qualitative evaluation of the PET image does not deliver the right answer. Beside due to a disease of the examined organ, a low uptake may be caused by a small amount of injected activity or a great body volume, so that a high percentage of the radiotracer is taken up by other body parts. In this situation the so-called standard uptake value (SUV) is helpful, which is defined as [1]:

$$\text{SUV} = \frac{\text{radioactivity concentration in the organ of interest (kBq/ml)}}{\text{injected radioactivity (MBq) / body mass (kg)}} \quad (7.1)$$

Assuming 1 ml is equivalent to 1g the SUV is without dimension. In clinical practice the SUV is the most often used parameter for a semiquantitative evaluation up a radiotracer accumulation. For example, a decreased SUV of FDG in a metastasis before and after treatment indicates the success of intervention.

Although the use of SUV is regarded as useful and is widespread, it is not sufficient to obtain a deeper insight into body functions in quantitative terms, i.e. how much does cerebral blood flow increase during stimulation or what percentage of neuroreceptors is blocked by a psychopharmaceutic? Table 1 presents a list of PET-radiopharmaceuticals and the corresponding functions.

To assess such functions based on quantified PET data different approaches have been developed. Although these approaches are very rarely applied in clinical practice, they have enabled clinical and basic research to *in vivo* analyse many aspects of human (patho-) physiology and biochemistry.

This chapter introduces into the different approaches leading from the radioactivity concentration quantified by PET to body functions.

7.2 The three components required for kinetic modelling

The general concept which is applied to evaluate a metabolic function in a quantitative way with PET is based on three components (Fig. 7.2):

1. the PET data which describe the spatial and temporal distribution of the radiopharmaceutical within the body and or an organ,
2. the simultaneously measured data about the temporal course of the radioactivity within the blood or plasma,
3. the metabolic model which yields a mathematical relationship between PET and blood data and the function of interest.

Ad1. Mostly the reconstructed PET images deliver time-activity data of a region or volume of interest (ROI or VOI) or of the entire image volume (Fig. 7.3 A). Some modelling procedures require just a single, so-called autoradiographic image resulting from a static PET acquisition or from summing up a temporal sequence of images (Fig. 7.3 B).

Ad2. Ideally the temporal course of the radioactivity within the blood or plasma is obtained from the artery supplying the organ to be examined. Therefore, this time-activity curve is also called input function. As it is generally not convenient or possible to obtain this function directly from the artery supplying the organ, one prefers to get blood samples from the radial or brachial artery. When measuring blood flow or blood volume it is sufficient to know the radioactivity concentration of the (whole) blood. Most applications, however, require the concentration of the radiotracer in the plasma, since the plasma concentration is decisive for the gradient of the radiotracer between the intra- and extravascular space. After centrifuging the blood samples plasma probes become available whose radioactivity is measured by a multi-probe well counter which has to be cross-calibrated in respect to the PET scanner. The cross-calibration ensures that the activity concentrations of both blood and PET image have the same unit kBq/cc. Often arterial blood sampling is regarded as too burdensome or not possible so that instead venous blood is withdrawn from, e.g. an antecubital vein. However, directly after the injection of the radiopharmaceutical there is a considerable discrepancy between arterial and venous radioactivity, so that the latter leads to an inaccurate input function – especially at early times after injection - and consequently to errors in the model analysis. Therefore, one heats the forearm by warm water or air etc. to arterialize the venous blood. Although this approach is not ideal, it may be acceptable, if

the heating leads to a venous oxygen content of more than 80%. If new radiopharmaceuticals are to be introduced and analysed one should apply arterial blood sampling first. Later one may check the errors by using arterialized venous blood sampling. Especially in neuroreceptor studies knowing the time-activity curve of the plasma is not sufficient, since most often the radiotracer is metabolized within the liver. In this case the plasma contains the originally injected radiotracer, but also the metabolised one – both labelled with the same positron emitter. To distinguish these two components plasma probes are analysed by thin-layer chromatography, for example, so that the time-activity curve of the plasma containing the non-metabolised radiotracer (also called free ligand) can be determined as input function (Fig. 7.4).

Ad 3. A general starting point to combine the three components shown in figure 7.2 is a balance. This balance considers the sum of fluxes of radioactivity into and out of an organ together with the change of radioactivity over the time within the organ. For this purpose the biological system to be analysed is divided into compartments. A compartment is a real or virtual volume in which substances are assumed to be instantaneously and homogeneously distributed. One of the mostly used compartment descriptions in PET is the simple 2-compartment model as presented in Fig. 7.5 A. It consists of a plasma (sometimes blood) compartment from which the radiopharmaceutical is transferred to the tissue compartment and vice versa. There may be further compartments (Fig. 7.5 B and C) whose role is explained later. Because the plasma compartment is always present, one often counts just the tissue compartments so that the models shown in Fig. 7.5 are also called 1-, 2-, and 3-tissue compartment models. The flux v from one compartment to another is mostly controlled by first order kinetics, i.e. the flux is proportional to the substance or radioactivity concentration c of the compartment from which v originates:

$$v = k\,c \qquad (7.2)$$

The proportionality factor k has the unit min^{-1} and is called rate constant. In the case of first order kinetics, k is a true constant. Using this relation the 1-tissue compartment model is expressed as in Fig 7.5 A. Commonly the transfer between the compartments is just indicated by the rate constants. Fig. 7.5 also contains the conventional order of indices used in the model setup in PET.

The corresponding mathematical equation with the balance of the fluxes as a function of time t reads

$$\frac{c_T(t)}{dt} = K_1 c_P(t) - k_2 c_T(t) \qquad (7.3)$$

$c_T(t)$ is the radioactivity concentration over time within the tissue as observed by PET. Mostly, one uses the capital K_1 instead of k_1, because it describes a constant of a clearance rate with the unit ml g^{-1} min^{-1} rather than a simple rate constant with the unit min^{-1}. At this point it is emphasized that the rate constants do not represent just a mathematical entity. As will be seen in the following they are the basic entities to obtain the quantified parameters of the observed biological function.

7.3 Kinetic analysis of a 1-tissue compartment model

The 1-tissue compartment model as defined Fig. 7.5 A and Eq. 7.2 is an often applied – sometimes simplifying - approach for radiopharmaceuticals whose uptake into the tissue is quite soon followed by the outwash back into blood vessels, i.e. they show reversible kinetics. Whereas the measured time functions $c_P(t)$ and $c_T(t)$ are known, the rate constants k_i which are the characterizing parameters of the compartment model are unknown and to be determined. For this purpose Eq. 7.2 must be solved. This can be achieved analytically or by numerical integration. The analytical solution of Eq. 7.2, which may be obtained with the help of the Laplace transform, reads:

$$c_T(t) = K_1 \int_0^t c_P(\tau) \bullet e^{-k_2 (t-\tau)} d\tau \qquad (7.4)$$

This equation represents the convolution integral of the input function $c_P(t)$ with the exponential term $e^{-k_2 t}$. The parameters k_i cannot directly be derived from Eq. 7.3. Instead they are numerically determined by fitting the left side of Eq. 7.4, i.e. the theoretical $c_T(t)$ to $c_T^{PET}(t)$ measured by PET. For this purpose one assumes initial values for K_1 and k_2 and using the measured $c_P(t)$ calculates a theoretical $c_T^{theor}(t)$, which most probably does not fit $c_T^{PET}(t)$. The comparison between $c_T^{theor}(t)$ and $c_T^{PET}(t)$ is commonly done by calculating the root square mean of the differences between the two functions:

$$RMS = \sqrt{\sum (c_T^{theor} - c_T^{PET})^2} \qquad (7.5)$$

This RMS is to be minimized so that so that $c_T^{theor.}(t)$ fits $c_T^{PET}(t)$ at its best. Since not all data have the same statistical quality, e.g. in case of short frames with increased noise, the squared differences of eq. 7.5 are often weighted by appropriate factors. If RMS is above a given threshold, the parameters k_i are varied by using a specific strategy and RMS is recalculated based the updated $c_T^{theor.}(t)$ - and so on. This iterative approach is called

nonlinear least square fitting and is visualized in Fig. 7.6. There are different strategies to vary the k_i in such a way so that *RMS* is minimized as fast as possible. The two approaches mostly applied in the kinetic analysis of PET data are the Simplex [2, 3] and the Marquardt-Levenberg [4, 5] algorithms. Finally, when $c_T^{theor.}(t)$ fits $c_T^{meas.}(t)$ the resulting k_i are regarded as those model parameters which describe the metabolic function in an optimum way. Fig 7.7 demonstrates the beginning and end of a curve fitting procedure using the program PMOD (Zürich; Switzerland) for biomedical image quantification [6].

K_1 characterizes the influx of the radiotracer into the tissue. The greater K_1 the faster the influx. Generally is

$$K_1 = E \bullet F\,, \tag{7.6}$$

the product of extraction fraction (E) and blood flow (F). The extraction fraction represents the difference between arterial and venous concentration divided by the arterial concentration, $(c_A - c_V)/c_A$. The more E approaches 1, i.e. c_V becomes very small, the more the parameter K_1 is governed by flow.

If E is 1, then K_1 represents the physiological function F so that Eq 7.4 can be written as

$$c_T(t) = F \int_0^t c_P(\tau) \bullet e^{-k_2(t-\tau)} d\tau \tag{7.7}$$

Fig. 7.8 shows the cerebral distribution of the cerebral blood flow (CBF) radiotracer [^{15}O]butanol and time-activity curves measured in a cortical region of interest (ROI). Although the images summed over a period of 2 min are very similar, the time-activity curve on the right hand side indicates both faster uptake and outwash of the radiotracer compared to left curve. The curve fitting based on Eq. 7.7 resulted in cortical CBF values of 61 ml/min/100g (left) and 174 ml/min/100g (right). This difference was caused by an experimental change of blood CO_2 from 30 to 60 mmHg [7].

There are kinetic processes, e.g. when studying reversible neurotransmitter ligands such as [^{11}C]raclopride, where the radiotracer uptake shows an equilibrium at time T_1 of a PET study so that

$$\frac{dc_T}{dt} = K_1 c_P - k_2 c_T = 0 \qquad \text{for } t = T_1 \tag{7.8}$$

and

$$\frac{K_1}{k_2} = \frac{c_T(T_1)}{c_P(T_1)} = DV \tag{7.9}$$

This ratio is a very often used metabolic parameter and is called the distribution volume (*DV*). In neurotransmitter receptor analysis *DV* is regarded as an indicator of the available

receptors. Instead of calculating *DV* as the ratio $c_T(T_1)$ over $c_P(T_1)$ one may determine DV via the fitting procedure which yields the K_1 and k_2. Even in cases, when a satisfying determination of the single k_i is not possible, the DV as their ratio shows a stable outcome.

7.4 The kinetic analysis of a 2- or 3-tissue compartment model.

The application of a 2-tissue compartment is adequate, if the radiotracer experiences a biochemical reaction after crossing from blood to tissue. In this case the first tissue compartment is regarded to contain the free radiotracer $c_F(t)$, the second tissue compartment represents the metabolized or bound tracer ($c_M(t)$ or $c_B(t)$) (see Fig. 7.5 B).
The following differential equations allow the mathematical analysis of 2-tissue compartment model:

$$\frac{dc_F}{dt} = K_1 c_P - (k_2 + k_3) c_F + k_4 c_M \qquad (7.11)$$

$$\frac{dc_M}{dt} = k_3 c_F - k_4 c_M \qquad (7.12)$$

The analytical solution for $c_T(t)$, which is $c_F(t)$ plus $c_M(t)$ as measured by PET, reads:

$$c_T{}^{PET}(t) = \frac{K_1}{a_2 - a_1} \int_0^t c_P(t-\tau) \bullet \left[(k_3 + k_4 - a_1) e^{-a_1 \tau} + (a_2 - k_3 - k_4) e^{-a_2 \tau} \right] d\tau \qquad (7.13a)$$

with

$$a_2, a_1 = (k_2 + k_3 + k_4) \pm \frac{1}{2} \sqrt{(k_2 + k_3 + k_4)^2 - 4 k_2 k_4} \qquad (7.13b)$$

The rate constants K_1 to k_4 can be obtained by a non-linear curve fitting approach as described in Sect. 7.3 and Fig. 7.6.
The analysis of the cerebral glucose metabolism with the help of FDG utilises the 2-tissue compartment model [8, 9]. In this case $c_P(t)$ and $c_F(t)$ contain the unchanged FDG whereas $c_M(t)$ represents the FDG-6-phosphate, which has undergone the hexokinase reaction. Knowing the rate constants K_1 to k_3 and neglecting k_4 [§] the local cerebral metabolic rate of glucose consumption (LCMRglc) is delivered by this operational equation:

[§] k_4 is neglected here, because it is much smaller than k_3.

$$LCMRGlc = \frac{c_P{}^{Glc}\left[c_T(T) - K_1 e^{-(k_2+k_3)T}\int_0^T c_P * (t) \bullet e^{(k_2+k_3)}dt\right]}{LC\left[\int_0^T c_P(t)dt - e^{-(k_2+k_3)T}\int_0^T c_P(t) \bullet e^{(k_2+k_3)}dt\right]} \quad (7.14)$$

$c_P{}^{Glc}$ represents the plasma glucose level and LC is a so-called lumped constant, which incorporates the biochemical difference between glucose and FDG. $c_T(T)$ is the FDG-concentration measured in a tissue of interest a time T. Whereas $c_P{}^{Glc}$ is the individual value of the subject investigated, standard literature values are used for *LC* and also for K_1 to k_3, if Eq. 7.10 is to be applied to all voxels of the FDG image recorded at time *T*. As explained below, individual constants K_1 to k_3 cannot reliably be determined by fitting the time-activity data of single voxels.

The 2-tissue compartment model is also applied in neuroreceptor analyses where the radiolabelled ligand is bound to the neuroreceptor ($c_B(t)$) (Fig. 7.9). As described in Sect. 7.5, the binding potential (BP) or the receptor affinity as interesting parameters can be derived from the rate constants calculated by curve fitting. Often, the neurotransmitter molecules do not only bind to the specific receptor, but also to other binding sites in an unspecific way. The latter binding becomes obvious when the specific binding is blocked by the injection of a specific antagonist prior to the PET measurement. To describe this biomedical behaviour a 3-tissue compartment (Fig. 7.5 C) is the appropriate model. Here the rate constants K_1 to k_6 are the parameters to be extracted from the kinetic PET study with the help of the fitting approach.

The fitting of four or even six rate constants suffers, however, from a general difficulty: the identifiability of the individual k_i. Often a perfect fit is observed, but the validity of the k_i must be questioned. There are several reasons for this uncertainty. The quality function RMS (k_i) may have local or relative minima in addition to the absolute minimum. Furthermore, several similar "absolute" minima may exist, as indicated in Fig. 7.10. Although a unique solution exists for the theoretical $c(t)$, this is not obvious for $RMS(k_i)$ which is influenced by errors and noise of both the measured PET and blood data. Especially, in models with 2- and 3-tissue compartments similar values of *RMS* are obtained for totally different sets of k_i depending on the initial values with which the fitting procedure is started. This situation is indicated in Fig. 7.10. In order to obtain the "true" rate constants, appropriate initial values should be selected and the most probable range of the k_i should be taken from literature or animal studies.

7.5 Model-based analysis of neuroreceptor metabolism

Although Fig. 7.5 C represents the appropriate model for neuroreceptor metabolism, this model is often simplified to obtain more reliable rate constants from the fitting procedure. Assuming a fast exchange between the two compartments of free and unspecifically bound (i.e. not bound to neuroreceptors) radiotracer, they may be combined to one compartment resulting in a 2-tissue compartment model.

Furthermore, sometimes all tissue compartments are lumped into one single tissue compartment. Although the fits for such a simplified model will probably be not ideal, one gets stable parameters K_1 and k_2 with their ratio equalling *DV*, which is an often used indicator for the availability of neuroreceptors. *DV* may be decreased due to a disease or because drugs are occupying (blocking) the neuroreceptors.

When applying and fitting the 2-tissue compartment model of neuroreceptor metabolism the binding potential *BP* of a radioligand can be calculated from:

$$BP = k_3 / k_4 \qquad (7.15)$$

BP represents the interplay between the two rate constants referring to the binding of the radioligand to and its release from the neuroreceptor.

If the concentration of the available neuroreceptors (B_{max}), which may be altered by a disease, is to be quantified, additional information is necessary. This can be achieved by two separate PET studies together with corresponding curve fitting procedures. In one study radioligand with high specific activity[&] is administered and a second study with low specific activity. This approach has been suggested by Mintun et al. [10], whose paper is recommended for further information. The double study delivers B_{max} and K_D. K_D is a measure of the affinity between the radioligand and the neuroreceptor and becomes smaller with higher affinity:

$$Affinity = 1 / K_D \qquad (7.16)$$

Furthermore, BP can be expressed as

$$BP = B_{max} / K_D \qquad (7.17)$$

K_D is very small for those radioligands, which bind strongly to the neuroreceptors. In this case *BP* becomes great. Assuming that K_D is not influenced by a drug or disease, *BP* is correlated with B_{max} and a measure for the maximum available neuroreceptors.

[&] The specific activity is the ratio between the mass of the radiolabelled ligand and the mass of the non-radiolabelled (cold) ligand.

There is another way to assess *BP* via the measurement of distribution volumes. For this purpose, in addition to the tissue with the specific binding by neuroreceptors a second so-called reference tissue is considered, which is devoid of neuroreceptors and expresses only unspecific binding. Often the cerebellum is regarded as a reference tissue. For both of these tissues, *DV* is determined resulting in DV_{Spec} and DV_{Ref}.

With

$$DVR = DV_{Spec} / DV_{Ref} \tag{7.18}$$

BP can be calculated from DVR:

$$BP = DVR - 1 \tag{7.19}$$

The present section does not aim at a comprehensive description of the many published suggestions to assess the outcome parameters of the neuroreceptor metabolism. Excellent reviews on the strategies to study the neuroreceptor metabolism have been written by Laruelle et al. [11] and Slifstein et al. [12]. An important paper entitled "Consensus Nomenclature for in vivo Imaging of Reversibly Binding Radioligands" has been published by Innis et al. [13]. Furthermore, the webpages of the Turku PET centre with a lot of additional information are recommended [14].

7.6 Parameter extraction by linearisation

The noise contained in the measured PET decreases, if ROIs are greater, and increases for small ROIs – especially, if an ROI comprises just a few voxels or even one voxel. The latter situation is true, if the radioactivity is to be converted voxel-by-voxel into a parametric image of the metabolic function to be studied. In this situation the nonlinear fitting procedure explained above should not be applied. Instead a linear approach must be chosen. For this purpose, the differential equation describing the model is rearranged with the result of a linear algebraic equation. Then, the outcome parameters can be determined for each voxel by a linear regression which supplies a unique solution.

The following first example aims at the calculation of parametric images of CBF, where a 1-tissue compartment model described by a differential equation as shown in Eq. 7.3 is applied. In this case K_1 is substituted by *F*. The linearisation is achieved first by integrating the differential model equation (Eq. 7.20) and second by appropriate rearranging (Eq. 7.21):

<<< I wish to have an reference of Yokoi et al, JNM 1993) for this linearization >>>

Yokoi T, Iida H, Itoh H, and Kanno I. A new graphic plot analysis for cerebral blood flow and partition coefficient with iodine-123-iodoamphetamine and dynamic SPECT validation studies using oxygen-15-water and PET. *J Nucl Med* 34(3): 498-

505, 1993

$$c_T(t) = F\int^t c_P(\tau)d\tau - k_2\int^t c_T(\tau)d\tau \qquad (7.20)$$

$$\frac{c_T(t)}{\int^t c_P(\tau)d\tau} = F - k_2\frac{\int^t c_T(\tau)d\tau}{\int^t c_P(\tau)d\tau} \qquad (7.21)$$

This equation defines the relationship for a straight line:

$$y(t) = F - k_2 x(t). \qquad (7.22)$$

Then, by calculating *y* and *x* for each time point *t* and by arranging *y(t)* over *x(t)* a plot such as that shown in Fig. 7.11 is obtained. If the straight part of this plot is fitted by a linear regression line, F results as the intercept of this line. To get a parametric image the linear regression procedure is applied voxel-by-voxel.

As mentioned above the *DV* is an important outcome parameter in neuroreceptor studies. If the kinetic model of a neuroreceptor ligand can be described by or simplified into a 1-tissue compartment model eq. 7.3 can be integrated and then rearranged into another linear equation:

$$\frac{\int^t c_T(\tau)d\tau}{c_T(t)} = -\frac{1}{k_2} + \frac{K_1}{k_2}\frac{\int^t c_P(\tau)d\tau}{c_T(t)} \qquad (7.23)$$

With $K_1/k_2 = DV$, the distribution volume of the neuroreceptor ligand can be obtained voxel-by-voxel as the slope of Eq. 7.23. Eq. 7.23 is similar[$] to that of the Logan [15] plot which is frequently used in the so-called graphical analysis of reversible neurotransmitter-receptor radioligands, i.e. radioligands, which are released from the neuroreceptor during the time of PET study. Furthermore, the derivation of the Logan plot includes also the 2-tissue compartment model for reversible radiotracers.

BP can be assessed on a voxel-by-voxel basis applying a suggestion of Logan et al.[16] to calculate *DVR* (see eqs. 7.17 and 7.18) via a linearization procedure. This approach does not require blood sampling, but uses a reference tissue such as the cerebellum as input function. The corresponding formula reads:

[$] Whereas the Logan plot considers the plasma volume fraction V_p, it is neglected here, so that the intercept is just $-1/k_2$.

$$\frac{\int^t c_T(\tau)d\tau}{c_T(t)} = Int + DVR\frac{\int^t c_{\mathrm{Re}\,f}(\tau)d\tau}{c_T(t)} \qquad (7.24)$$

At this point an often used reference tissue approach introduced by Lammertsma and Hume [17] may be indicated: the simplified reference tissue model. Although originally developed for the evaluation of ROI data, it can deliver parametric images when applying calculations voxel-by voxel with basic functions rather than linearization as suggested by Gunn et al. [18]. Another famous linearisation approach is that of the Patlak [19] plot which is applied for 2-tissue compartment models with k_4 equal zero, e.g. in the case of irreversible binding:

$$\frac{c_T(t)}{c_P(t)} = V_o + \frac{K_1 \cdot k_3}{k_2 + k_3}\frac{\int^t c_P(\tau)d\tau}{c_P(t)} \qquad (7.25)$$

The slope $(K_1\ k_3)/(k_2 + k_3)$ represents the influx rate of the radiotracer into the irreversible compartment. In the case of FDG, the phosphorylated FDG is nearly completely trapped in such a compartment, so that the rate constant k_4 can be neglected. The application of Eq. 7.10 for obtaining a parametric image of LCMRglc requires the use of general, non-individual rate constants. The Patlak plot opens the way to an image of LCMRglc calculated voxel-by-voxel considering individual rate constants, when the slope determined by Eq. 7.25 is utilized in the following formula suggested by Phelps et al. [8]:

$$LCMRGlc = \frac{c_P^{\ Glc}}{LC}\frac{K_1 \cdot k_3}{k_2 + k_3} \qquad (7.26)$$

7.7 MR-PET protocol for neuroreceptor studies

Fig. 7.12 describes a possible protocol of a simultaneous MR-PET study. The PET investigation uses a reversible radioligand and a bolus-infusion [20] scheme for administering the radioligand. In this way an equilibrium between tissue and input function can be achieved so that Eq. 7.9 can be applied, i.e. the DV_{Spec} in the specific target ROI and DV_{Ref} in the reference ROI must be measured:

With

$$DV_{Spec} = c_{Spec}(t)/c_P(t) \quad and \quad DV_{Ref} = c_{Ref}(t)/c_P(t) \qquad (7.27)$$

one gets

$$DVR = DV_{Spec} / DV_{Ref} = c_{Spec}(t) / c_{Ref}(t) \quad (7.28)$$

so that an input function is not required and the only necessary data are the activity concentrations $c_{Spec}(t)$ and $c_{Ref}(t)$ measured by PET.

One aim of such a study may be a change of DV_{Spec} caused by a challenge or stimulation in the second part of the acquisition. So one can compare DVR without and with challenge. Using Eq. 7.19 changes in *BP* follow directly from changes in *DVR*.

While PET gives information about changes of receptor binding due to a challenge, MRI may supply additional and complementary data. For example, as indicated in Fig. 7.12 about CBF with arterial spin labelling (ASL) or about the concentration of neurotransmitters with magnetic resonance spectroscopy (MRS). There are uncertainties, whether the uptake of radioligands is flow-dependent [21]. Therefore, MRI-based measurements of CBF are to ensure that changes of *DVR* are caused by altered neuroreceptor metabolism and not by altered CBF.

References

1. K. R. Zasadny and R. L. Wahl, *Radiolog*, 1993, **189**, 847.
2. G. Dantzig, *Programming in a linear structure*, U.S. Air Force Comptroller, USAF, Washington, D.C., 1948.
3. J.A. Nelder and R. Mead, *Comput. J*., 1965, **7**, 308.
4. D.W. Marquardt, *J. Soc. Indust. Appl. Math.*, 1963, **11**, 431.
5. K. Levenberg, *Quart. Appl. Math*., 1944, **2**, 164.
6. C. Burger and A. Buc, *J. Nucl. Med.*, 1998, **38**, 1818.
7. L.J. Kemna, S. Posse, H. Herzog, V.G. Kiselev, S. Wiese, D. Gembris and L. Tellmann, *NeuroImage*, 1999, **9**, No. 6, Part 2, S281.
8. M.E. Phelps, S.C. Huang, E.J. Hoffman, C. Selin, L. Sokoloff, D.E. Kuhl, *Ann. Neurol.*, 1979, **6**, 371.
9. M. Reivich, D. Kuhl, A. Wolf, J. Greenberg, M. Phelps, T. Ido, V. Casella, J. Fowler., E. Hoffman, A. Alavi, P. Som and L. Sokoloff, *Circ. Res*., 1979, *44*, 127.
10. M.A. Mintun, M.E. Raichle, M.R. Kilbourn, G.F. Wooten and M.J. Welch. 1984, A quantitative model for the in vivo assessment of drug binding sites with positron emission tomography. *Ann. Neurol.*, 1984, **15**, 217.
11. M. Laruelle, M. Slifstein and Y. Huang,. *Methods*, 2002, **27**, 287.
12. M. Slifstein and M. Laruelle. *Nucl. Med. Biol.*, 2001, **28**, 595.
13. R.B. Innis and 24 co-authors, *J. Cereb. Blood Flow Metab*., 2007, **27**, 1533.
14. http://www.turkupetcentre.net/petanalysis/tags.html#Modeling
15. J. Logan, J.S. Fowler, N.D. Volkow, A.P. Wolf, S.L. Dewey, D.J. Schlyer, R.R. MacGregor, R. Hitzemann, B. Bendriem, S.J. Gatley, and D.R. Christman, *J. Cereb. Blood Flow Metab*., 1990, **10**, 740.
16. J. Logan, J.S. Fowler, ND. Volkow, G.J. Wang, Y.S. Ding and D.L. Alexoff, *J Cereb Blood Flow Metab*. 1996, **16**, 834.
17. A.A. Lammertsma and S.P. Hume, *NeuroImage*, 1996, **4**, 153.
18. Gunn RN, Lammertsma AA, Hume SP and Cunningham VJ, *Neuroimage*, 1997, **6**, 279.
19. C.S. Patlak, R.G. Blasberg, and J.D. Fenstermacher, (March 1983). *J. Cereb. Blood Flow Metab*., 1983, **3**, 1.
20. R.E. Carson, M.A. Channing, R.G. Blasberg, B.B. Dunn, R.M. Cohen, K.C. Rice and P. Herscovitch, *J. Cereb. Blood Flow Metab*., 1993, **13**, 24.
21. N.M. Alpert, R.D. Badgaiyan, E. Livni and A.J. Fischman, *Neuroimage*, 2003, **19**, 1049.

Table 1 - Using appropriate kinetic models different physiological and metabolic functions can be derived from images of corresponding PET-radiopharmaceuticals

PET-Radiopharmaceutical	Function
^{18}F-Fluordeoxyglucose	Glucose consumption
^{15}O-Water	Perfusion
^{15}O-Butanol	Perfusion
^{15}O-Oxygen	Oxygen consumption
^{15}O-CO	Blood volume
^{11}C-Raclopride	Binding potential to and density of dopamin receptors
^{11}C-Flumazenil	Binding potential to and density of benzodiazepine receptors
^{18}F-Altanserin	Binding potential to and density of serotonin receptors
^{11}C-Carfentanil	Binding potential to and density of opoid receptors

Table 2 – Overview of different compartment models and analysis (plot) tools with the necessary input dada and the achievable outcome parameters. IF= input function. The other abbreviations are explained in the text

Model / Analysis Tool	Necessary Data	Outcome
1-tissue compartment (example [^{15}O]water or [^{11}C]raclopride simplified from 2-tissue compartment	- Quantified PET data - IF ($c_p(t)$)	K_1 and k_2 F, if E is known or assumed 1. $DV=K_1/k_2$
2-tissue compartment (example FDG or simplification of neurotransmitter 3-tissue compartment, when free and unspecific compartments are lumped into one)	- Quantified PET data - IF ($c_p(t)$) - FDG: plasma glucose level of subject and Lumped constant (standard value)	K_1 to k_4 FDG: general $LCMR_{glc}$ (if $k_4=0$) Neurotransmitters: $BP=k_3/k_4$ B_{max} and K_D (high and low affinitiy study)
2-tissue compartment for neurotransmitter	- Quantified PET data - Reference tissue as IF	$DVR=DV_{spec}/DV_{ref}$ BP=DVR-1
Logan Plot (reversible tracers)	- Quantified PET data - IF ($c_p(t)$)	DV (slope)
Logan Plot with reference tissue	- Quantified PET data - Reference tissue as IF	DVR (slope) BP=DVR-1
Patlak Plot (irreversible tracers)	- Quantified PET data - IF ($c_p(t)$)	FDG: $LCMR_{glc}$ (if $k_4=0$)
Analysis of reversible neurotransmitter with bolus-infusion-protocol	- Quantified PET data - IF ($c_p(t)$)	DV_{spec} at equilibrium DV_{ref} at equilibrium $DVR=DV_{spec}/DV_{ref}$

Figure Captions

Figure 7.1

Qualitative images comparing the cerebral uptake of ^{18}F-fluoro-deoxyglucose (FDG) in a normal volunteer and a patient with Alzheimers disease. The red arrows mark the loss of neurons in the occipitotemporal cortex which in an indicator for this kind of dementia.

Figure 7.2

Flowchart for the calculation of metabolic functions. Quantitative dynamic or static PET data and time-activity data of the radioactivity concentration in the blood, which are cross-calibrated to each other, are required as input into a mathematical metabolic model.

Figure 7.3

Quantitative PET data of ^{18}F-fluoro-deoxyglucose (FDG) presented as a dynamic sequence of images ranging from shortly after injection until 55 min, when a nearly constant level of tracer of uptake is reached (A). Averaged image of cerebral FDG uptake by summing images of the dynamic sequence from 30 to 55 min (B, green arrow)). In order to obtain a time-activity of the cerebral FDG dynamics a region of interest (ROI) is defined on the averaged image and then transferred to the dynamic images (pink arrow). The time-activity curve is obtained by integrating the radioactivity concentration of each image within the ROI and by plotting the integrated values over time (C) .

Figure 7.4

Time-activity curves of a PET radiotracer for neuroreceptor studies measured in blood, in plasma and as free ligand, i.e. unmetabolised radiotracer.

Figure 7.5

The mostly used compartment models in PET. (A) 1-tissue compartment model applied for flow radiotracers or for the simplified description of models of reversibly bound

neuroreceptor ligands. (B) 2- tissue compartment model applied for FDG and neuroreceptor ligands. (C) 3- tissue compartment model applied for neuroreceptor ligands, if a compartment for the unspecifically bound radiotracer is to be considered.

Figure 7.6

Block diagram indicating the algorithm for iterative curve fitting.

Figure 7.7

Example for iterative curve fitting of a 1-tissue compartment model using the program PMOD (Zürich; Switzerland) for biomedical image quantification. The left plot shows the start of the fitting procedure with a great discrepancy between the measured kinetic PET data and the theoretical model solution, for which initial values for K_1 and k_2 were assumed. The right plot documents the end of the fitting procedure with a satisfying match between measured PET data and theoretical curve

Figure 7.8

Images of the cerebral blood flow (CBF) radiotracer ^{15}O-butanol and time-activity curves measured in a cortical region of interest (ROI). Whereas the images are very similar, the time-activity curve on the right hand side indicates both faster uptake and outwash of the radiotracer compared to left curve. Correspondingly the curve fitting based on Eq. 7.7 resulted in cortical CBF values of 61 ml/min/100g (left) and 174 ml/min/100g (right). This difference was caused by an experimental change of blood CO_2 from 30 to 60 mmHg [7].

Figure 7.9

Scheme of the uptake and binding of a radioligand with an affinity to neuroreceptors. The radioligand enters the extracellular space (F) at the synaptic gap from the blood via the blood brain barrier (BBB) and part of it binds to neuroreceptors at the postsynaptic membrane. Other neuroreceptors are occupied by internal neurotransmitter molecules, which are released from the presynaptic neuron. Fig. 7.5 B and Eqs. 7.11 and 7.12 present the corresponding compartment model and mathematical description. If appropriate F may be subdivided in compartments with unbound and unspecifically (not to neuroreceptors) bound radioligand (see Fig. 7.5 C).

Figure 7.10

Top: A plot of the root mean square (RMS) values over the rate constants k_i demonstrates that the fitting procedure may end in different minima dependent on the initial values of k_i.

Bottom: The curve fitting procedure of a simulated 3-tissue compartment model produces very different sets of k_i in spite of nearly same RMS.

Figure 7.11

Example of determining CBF by linear regression with application of Eq. 7.22.

Figure 7.12

Possible protocol of a simultaneous MR-PET study to assess different aspects of neuroreceptor metabolism.

Figure 7.1

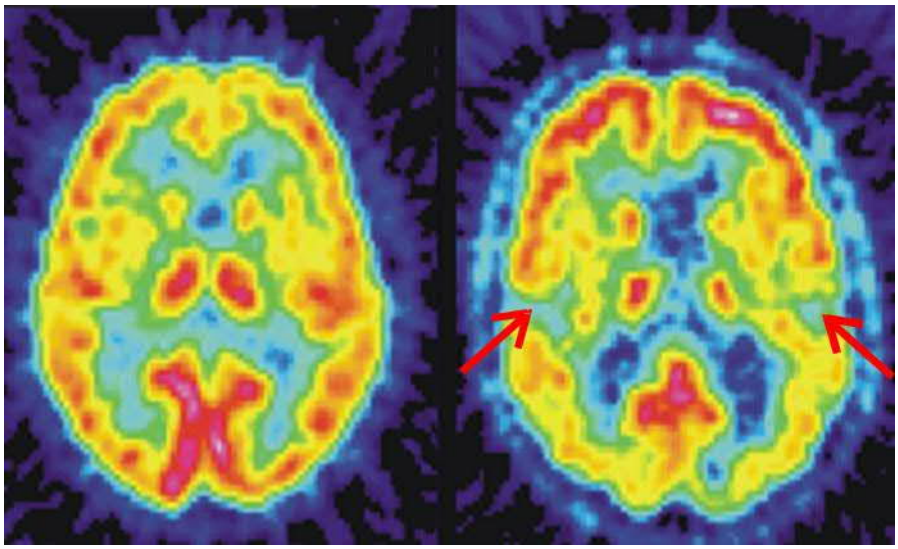

Figure 7.2

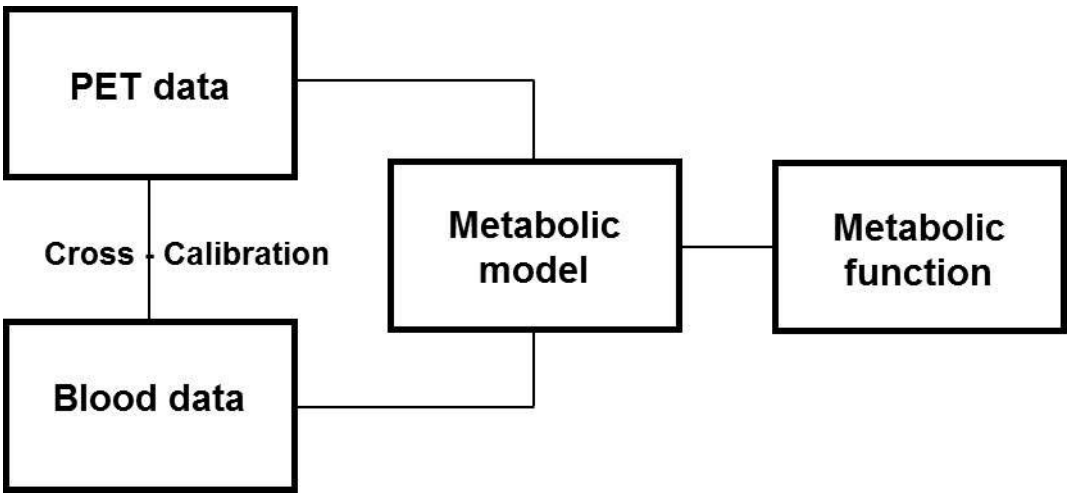

Figure 7.3

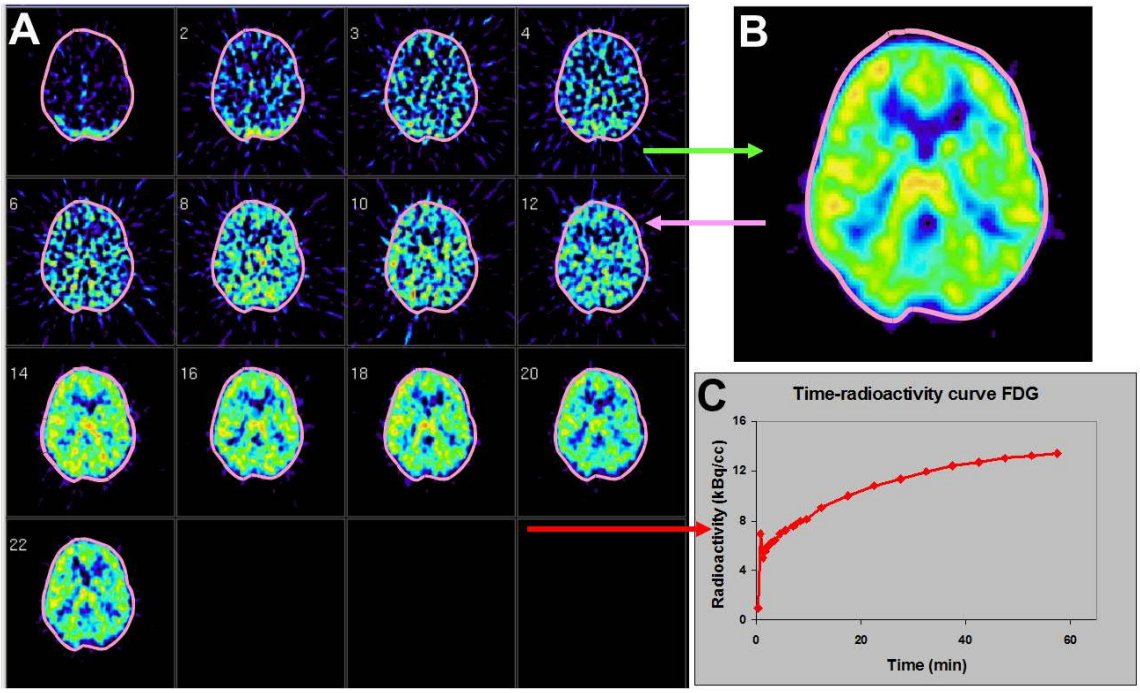

Figure 7.4

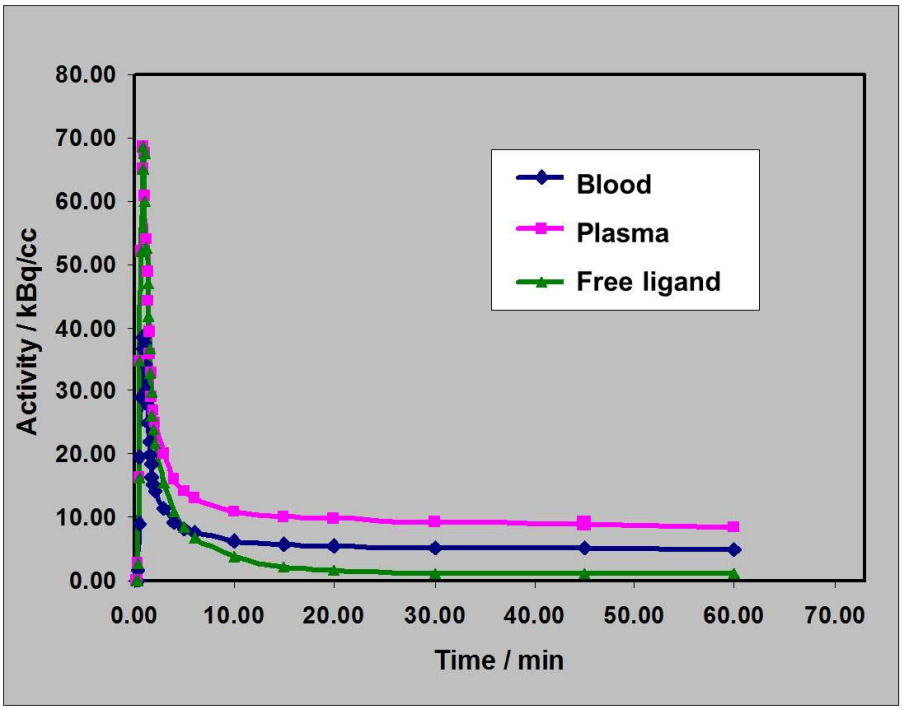

Figure 7.5

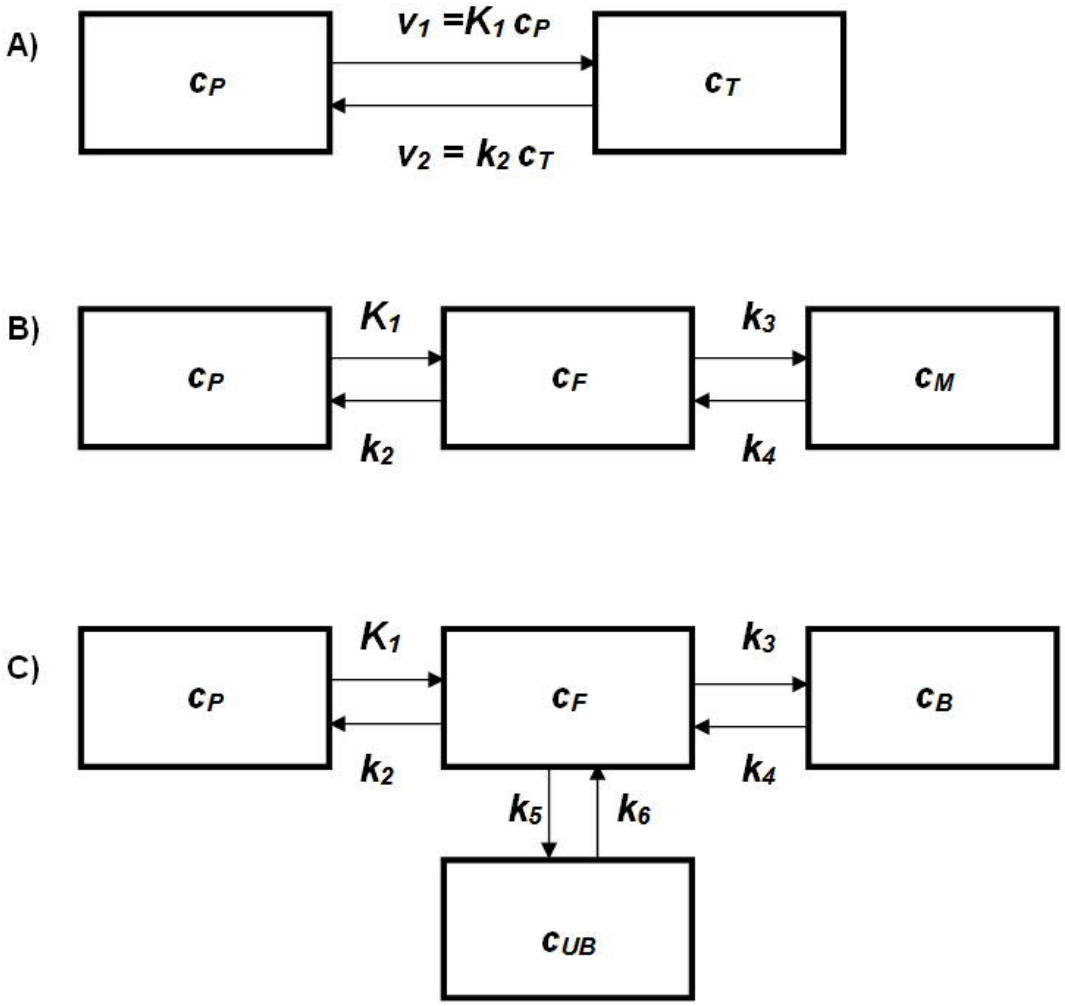
A)
c_P
$v_1 = K_1 c_P$
c_T
$v_2 = k_2 c_T$
B)
c_P
K_1
k_2
c_F
k_3
k_4
c_M
C)
c_P
K_1
k_2
c_F
k_3
k_4
c_B
k_5
k_6
c_{UB}

Figure 7.6

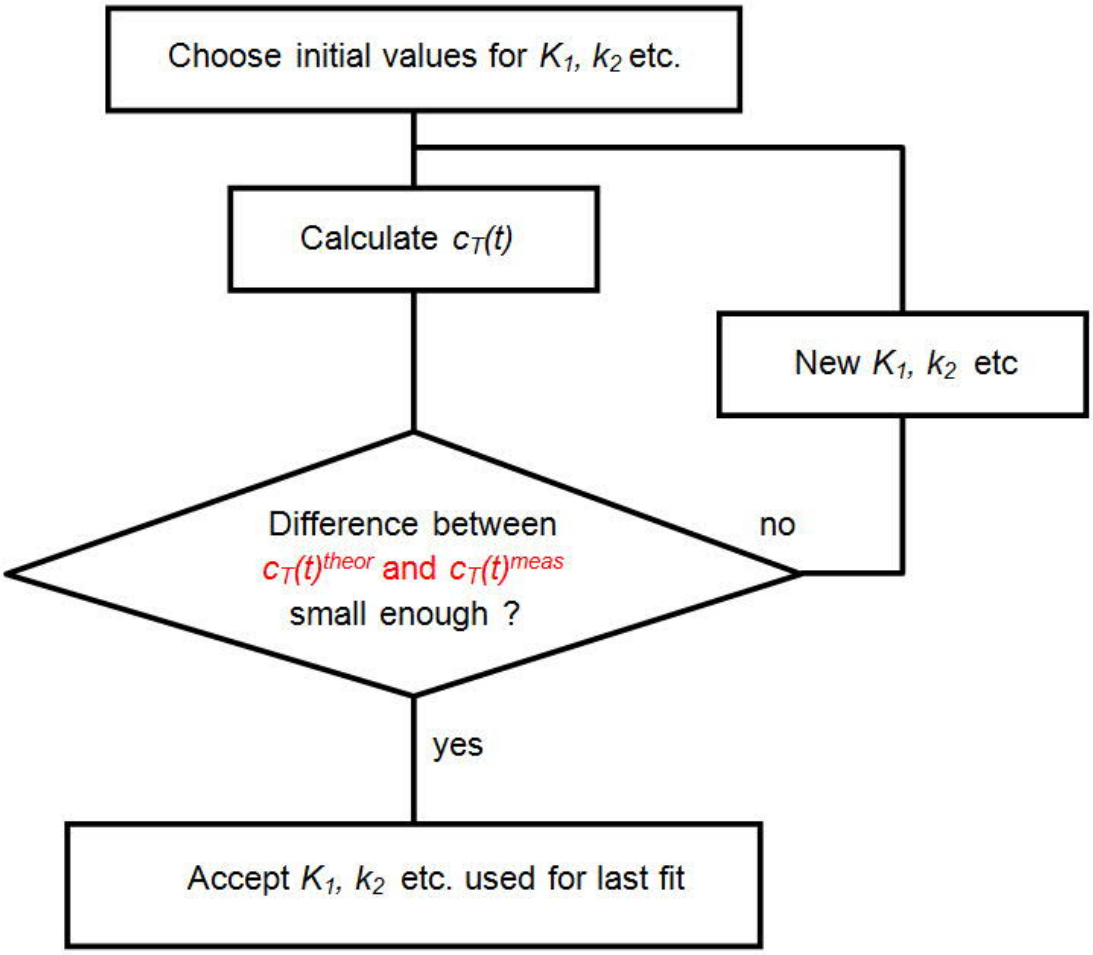

Figure 7.7

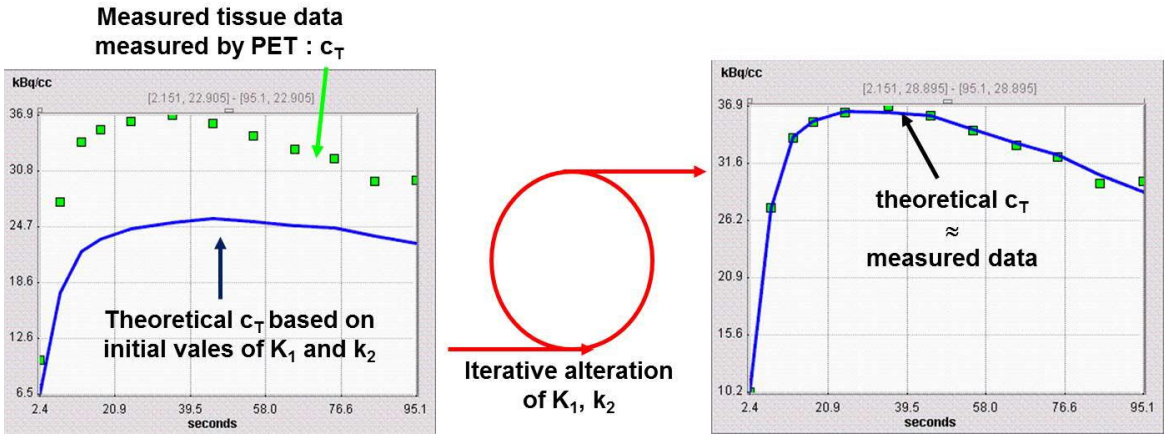

Figure 7.8

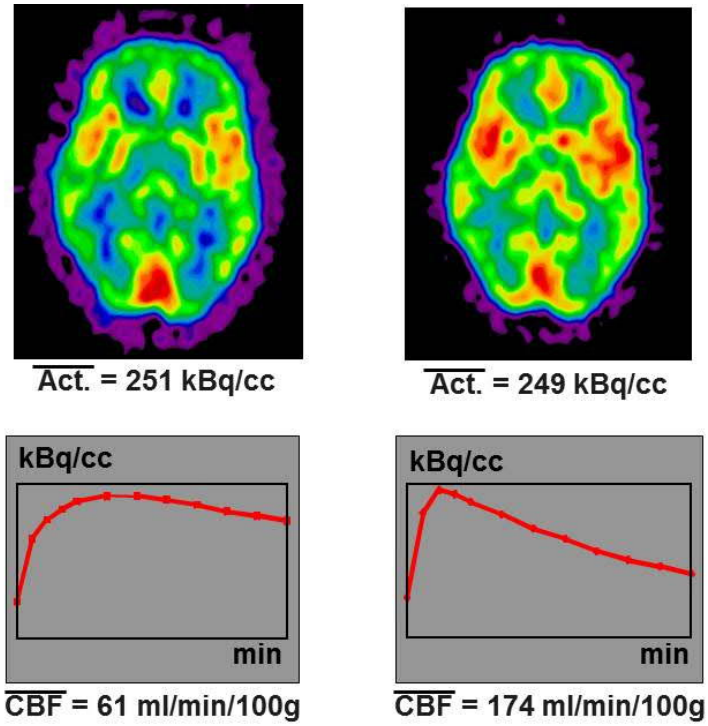

Figure 7.9

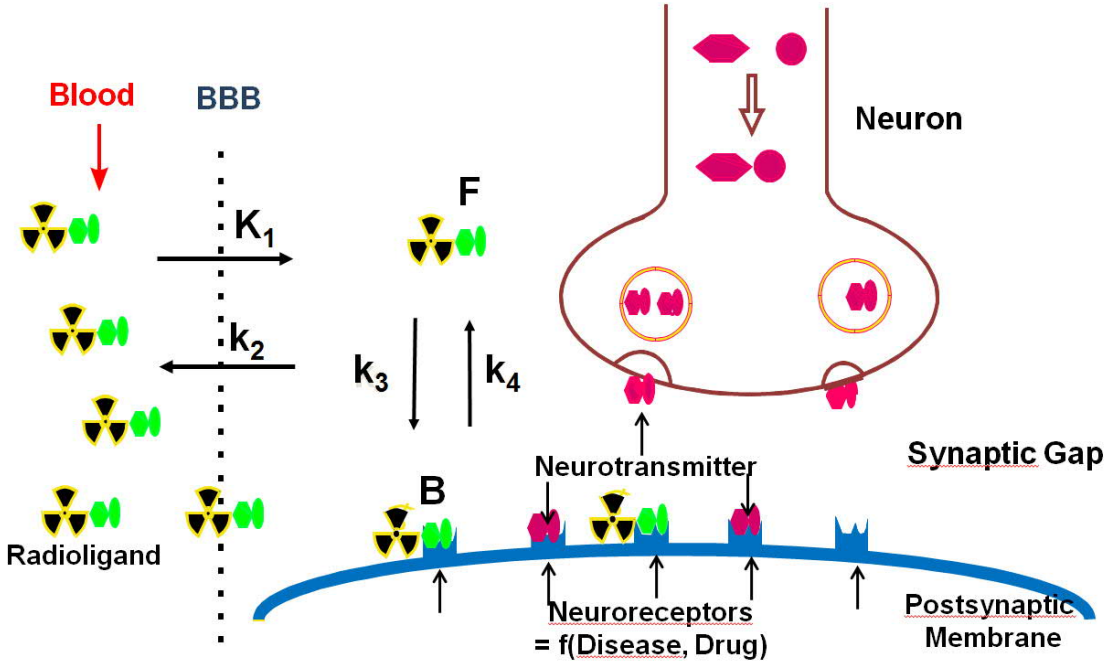

Figure 7.10

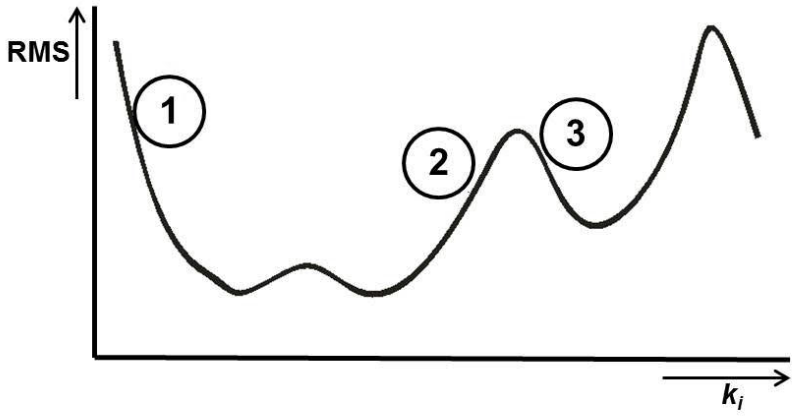

Parameter	K_1	k_2	k3	k4	k5	k6	
Given	**0.107**	**0.201**	**0.201**	**0.060**	**0.029**	**0.026**	RMS
Fit 1	0.110	0.171	0.000	0.652	0.191	0.058	10.351
Fit 2	0.152	0.554	0.231	0.048	0.181	0.045	10.281
Fit 3	0.112	0.186	0.003	0.058	0.203	0.058	10.279

Figure 7.11

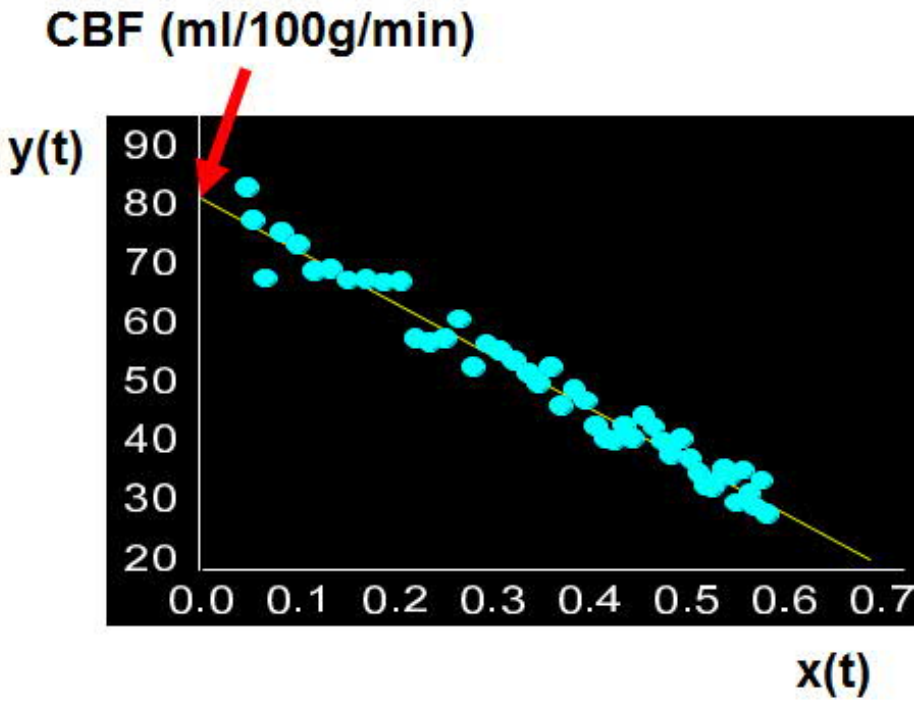

Figure 7.12

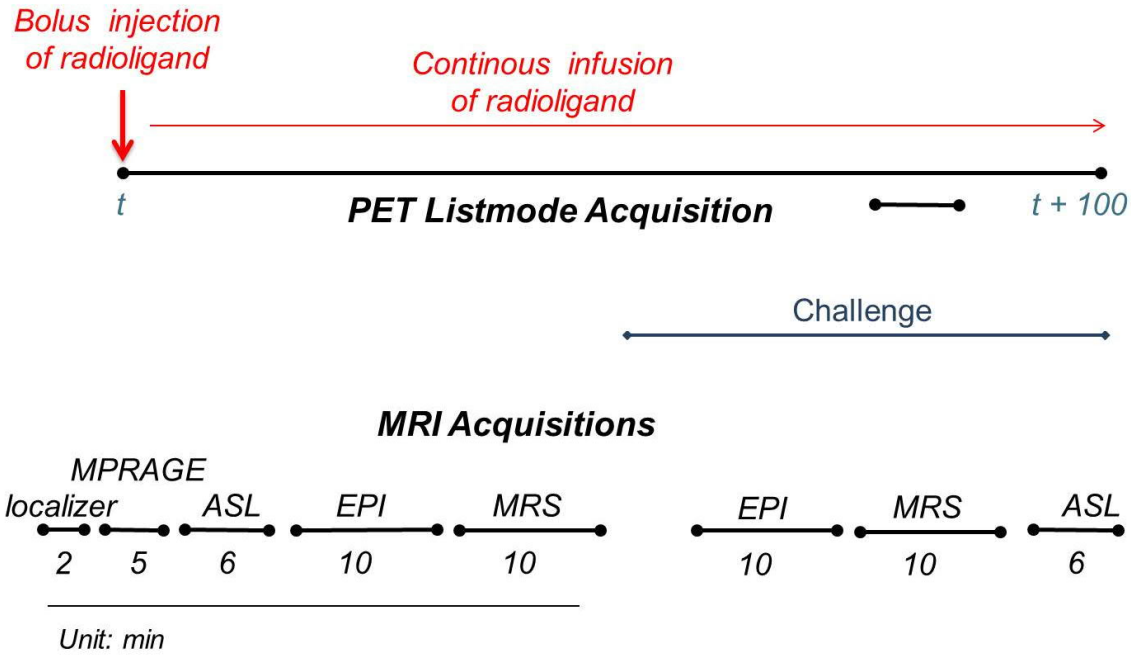
Bolus injection of radioligand
Continous infusion of radioligand
t
PET Listmode Acquisition
t + 100
Challenge
MRI Acquisitions
MPRAGE localizer
ASL
EPI
MRS
EPI
MRS
ASL
2
5
6
10
10
10
10
6
Unit: min